



UNIVERSITY OF LEEDS

This is a repository copy of *The rheology of polyvinylpyrrolidone-coated silica nanoparticles positioned at an air-aqueous interface*.

White Rose Research Online URL for this paper:  
<http://eprints.whiterose.ac.uk/134328/>

Version: Accepted Version

---

**Article:**

Yu, K, Zhang, H, Biggs, S et al. (3 more authors) (2018) The rheology of polyvinylpyrrolidone-coated silica nanoparticles positioned at an air-aqueous interface. *Journal of Colloid and Interface Science*, 527. pp. 346-355. ISSN 0021-9797

<https://doi.org/10.1016/j.jcis.2018.05.035>

---

© 2018 Elsevier Inc. This manuscript version is made available under the CC-BY-NC-ND 4.0 license <http://creativecommons.org/licenses/by-nc-nd/4.0/>.

**Reuse**

This article is distributed under the terms of the Creative Commons Attribution-NonCommercial-NoDerivs (CC BY-NC-ND) licence. This licence only allows you to download this work and share it with others as long as you credit the authors, but you can't change the article in any way or use it commercially. More information and the full terms of the licence here: <https://creativecommons.org/licenses/>

**Takedown**

If you consider content in White Rose Research Online to be in breach of UK law, please notify us by emailing [eprints@whiterose.ac.uk](mailto:eprints@whiterose.ac.uk) including the URL of the record and the reason for the withdrawal request.



[eprints@whiterose.ac.uk](mailto:eprints@whiterose.ac.uk)  
<https://eprints.whiterose.ac.uk/>

# The rheology of polyvinylpyrrolidone-coated silica nanoparticles positioned at an air-aqueous interface

Kai Yu<sup>1</sup>, Huagui Zhang<sup>1</sup>, Simon Biggs<sup>2</sup>, Zhenghe Xu<sup>3</sup>, Olivier J. Cayre<sup>1</sup>, and David Harbottle<sup>1\*</sup>

<sup>1</sup> School of Chemical and Process Engineering, University of Leeds, UK

<sup>2</sup> School of Chemical Engineering, The University of Queensland, Australia

<sup>3</sup> Department of Chemical and Materials Engineering, University of Alberta, Canada, and Department of Materials Science and Engineering, Southern University of Science and Technology, Shenzhen, China

## ABSTRACT

Particle-stabilized emulsions and foams are widely encountered, as such there remains a concerted effort to better understand the relationship between the particle network structure surrounding droplets and bubbles, and the rheology of the particle-stabilized interface. Poly(vinylpyrrolidone) coated silica nanoparticles were used to stabilize foams. The shear rheology of planar particle-laden interfaces were measured using an interfacial shear rheometer and the rheological properties measured as a function of the sub-phase electrolyte concentration and surface pressure. All particle-laden interfaces exhibited a liquid-like to solid-like transition with increasing surface pressure. The surface pressure-dependent interfacial rheology was then correlated to the formed micron-scale structures of the particle-laden interfaces which were imaged using a Brewster angle microscopy. With the baseline knowledge established, foams were prepared using the same composite particles and the particle network structure observed using cryo-SEM. An attempt has been made to correlate the two structures observed at a planar interface and that surrounding a bubble to elucidate the likely rheology of the bubble stabilizing particle network. Independent of the sub-phase electrolyte concentration, the resulting rheology of the bubble stabilizing particle network was strongly elastic and appeared to be in a compression state at the region of the L-S phase transition.

## 1. INTRODUCTION

2D colloid assembly at gas – liquid or liquid – liquid interfaces of particle-stabilized foams and emulsions have been progressively utilized to produce novel, functional products and materials.[1-4] An increase in the number of applications has resulted from the significant research interests in particle assembly over the past few decades.[5, 6] We now have a sufficiently detailed understanding of these systems to allow us to fine tune their properties.[5, 7, 8] This precise control on particle assembly at interfaces can now be used to design-in performance characteristics, i.e. structure – property relationship control.[9, 10] In the simplest case the range of particle structures can be bound by the degree of dispersion, with interfacial and bulk properties significantly different when considering particle-laden interfaces of highly dispersed and close packed assembly.[11]

The potential for a particle to reside at a liquid-liquid interface is highly dependent on the interaction forces between the particle and interface,[12] and the particle wettability.[13-16] While particle interactions in a single phase are well characterized, the asymmetric alignment of particles at an interface between two immiscible liquids of contrasting polarity introduces added complexity which contributes to the overall arrangement of the particle assembly.[17] The main forces contributing to the particle assembly include colloidal (DLVO), capillary, monopolar and dipolar interactions. Since the dipolar and dispersion forces are a function of the total surface area exposed to the non-aqueous and aqueous phases, respectively, the overall interaction energy becomes very sensitive to the particle wettability.[18]

Control on particle assembly offered by the particle wettability has been demonstrated in several recent studies.[13-16] For hydrophilic particles, particle assembly is governed by the interaction forces mediated through the aqueous phase. Since the particle repulsion is weak, hydrophilic particles have a tendency to form particle clusters which have been observed to densify through the addition of electrolyte, and as a function of time.[18] Similar to the particle aggregation kinetics observed in the bulk, particle aggregation at the liquid-liquid interface follows the diffusion-limited (DLCA), or reaction-limited cluster aggregation (RLCA) kinetics to form low density or high density gel-like networks, respectively.[10, 19] For strongly hydrophobic particles,

well ordered, crystalline structures have been observed when deposited at a liquid-liquid interface,[20] with the long-range Coulomb interaction dominating the particle-particle repulsion.

Particle assembly can also be influenced by the number of particles residing at the liquid-liquid interface.[9, 21] The contribution of particle networks to the rheological properties of the liquid-liquid interface is significant, with the lateral mobility of particles and particle domains governing the stability of droplets and bubbles.[22-24] The mobility of the particle-laden interface was shown to be a function of the particle coverage and the applied shear at the interface.[25] At relatively low particle concentrations, the lateral displacement force is low and the particles migrate in slip layers. At slightly higher particle concentrations, the lateral displacement force also remains low but mobility is frequently observed through the rotation of particle domains due to the influence of neighbouring particles. The force required to laterally displace particles at an interface increases dramatically as the 2D close-packed assembly is approached ( $\Phi \sim 75\%$ ).[26] This increase in the lateral displacement force correlates to a sudden increase in the interfacial shear rheology.[9] At very high particle concentrations the shear deformation of the interface is highly constrained, leading to ‘jamming’ of the particle domains, restricting mobility as the interface response becomes solid-like.[9, 27] As a result, the rigid particle network remains intact and inhibits droplet coalescence when two liquid interfaces (droplets or bubbles) approach.[23] The critical particle concentration for network jamming is dependent on the attractive potential, with strong attraction between particles leading to the formation of a space-spanning, contiguous particle assembly of increased shear viscosity at significantly lower particle surface coverages ( $\Phi \sim 40\%$ ).[10, 19] The liquid-like to solid-like boundary has been shown to strongly correlate to the decreased probability of droplet coalescence.[23] In a solid-like state, mobility of the particle assembly can only be achieved once the particle assembly is ruptured after the sustained stress exceeds the interfacial shear yield stress of the particle-laden interface.[22, 28]

The surface shear rheology dependence on particle wettability has been considered by Safouane et al. using  $\sim 200$  nm amorphous fumed silica particle aggregates.[29] The aggregate wettability was controlled by adjusting the SiOH surface content. For weakly hydrophobic particles the surface shear elasticity ( $G'$ ) was unmeasurable and close to the sensitivity limit of the measurement

technique. For weak particle networks Van Hooghten[30] emphasized that care should be taken when interpreting the viscoelastic properties of particle-laden films because the geometry inertia can lead to erroneous behaviour. As particles partition more strongly at the air-water interface the contribution from  $G'$  emerges and a strongly elastic interface eventually formed with long-range attraction attributed to hydrophobic and capillary forces.[29] As a function of particle concentration and strength of particle-particle contact, Zhang et al.[19] highlighted both one-step and two-step yielding mechanisms for particle-laden interfaces. Beyond the fluid-solid transition, weakly aggregated particle networks exhibited one-step yielding with two-step yielding observed with increasing elasticity of the particle-laden film. The mechanism for yielding was attributed to the particle dynamics arrested first from attraction induced bonding bridges and then from the cage effect of particle jamming.

A second mode of interface deformation that is often discussed in relation to bubble or droplet stability is the dilatational rheological term (elasticity). This mode of deformation considers the expansion and contraction of interfacial area. While it is considered to be a dominant stabilization mechanism for surfactants, relatively few studies have considered the dilatational rheology of particle-stabilized interfaces. In the same study by Safouane et al.[29] the compression elastic modulus was shown to predominantly exceed the compression loss modulus over a range of surface coverages and particle wettabilities. This dominance of elastic over viscous contributions has been seen for a range of particle systems. [12, 31-34] While the dilatational elasticity is a useful parameter to define conditions under which bubbles or droplets can resist coarsening, recent research has shown that for droplet coalescence it is the shear rheology that governs stability, with interfaces preferring to shear under an applied load, i.e. the shear viscoelastic moduli are smaller than the dilatational viscoelastic moduli.[23, 35]

In our recent study, polymer-coated nanoparticles were shown to be effective foam stabilizers, with the foam stability dependent on the aqueous phase electrolyte concentration.[22] The current study develops those initial findings to better understand the structure-rheology relationship for polymer-coated nanoparticles deposited at the planar air-water interface. Using techniques such as Brewster Angle Microscopy (BAM) and pressure-modulated interfacial shear rheology, we are

able to directly correlate the mechanical properties of the particle-laden interface to its structure. We extend our observations to make some initial assessment about the rheology of particle-laden interfaces surrounding foam bubbles by correlating the structures observed at 2D planar and bubble interfaces.

## 2. MATERIALS AND METHODS

**2.1 Materials** A Ludox AS40 silica nanoparticle sample was supplied by Sigma-Aldrich (UK) as a 40 wt% aqueous suspension. Poly(vinylpyrrolidone) (PVP, 40 kDa) was supplied by Alfa Aesar (UK) and used without further purification. Prior to its use the silica particle suspension was diluted to 10 wt% using Milli-Q water and then ion exchanged using Amberlite IRN 50 resin (Alfa Aesar, UK) to remove excess  $\text{SO}_4^{2-}$  counter-ions. The particle diameter measured using a Malvern ZetaSizer Nano ZS (Malvern Instruments, UK) was  $\sim 34$  nm with a PDI of 0.14. Milli-Q water with a resistivity of  $18.2 \text{ M}\Omega\cdot\text{cm}$  was used throughout the study and sodium sulphate (99+%, A.C.S. R, Sigma Aldrich, UK) used to adjust the electrolyte concentration.

The polymer-coated composite particles were prepared using a simple one-step adsorption process.[22] The successful formation of the composite particles was verified by transmission electron microscopy (FEI Tecnai TF20, UK) and thermo-gravimetric analysis (Q-500 TA Instruments, USA), see Yu et al. for detailed analysis of the prepared composite particles.[22] The TEM images (Fig. S1) showed a core-shell structure and the mean hydrodynamic diameter ( $D_h$ ) of the composite particles in Milli-Q water was 52 nm, indicating that the average thickness of the hydrated polymer shell was approximately  $\sim 9$  nm. The PVP surface coverage ( $\Gamma$ ) on the silica nanoparticles was determined to be  $\sim 0.9 \text{ mg/m}^2$  as measured by TGA.[22] Our previous study confirmed the stability of PVP to water rinse-off, with negligible mass removed following adsorption on silica.[49] For the current experimental conditions the adsorbed PVP was shown to be stable to the sample washing procedure outlined in Yu et al.[22] and throughout the duration of the study.

## 2.2 Characterization of particle-laden interfaces

2.2.1 *Π*-A Isotherms Surface pressure–area ( $\Pi - A$ ) isotherms of deposited particle layers were studied using an air-liquid Langmuir trough (Biolin Scientific, Sweden), with a maximum trough area of 280 cm<sup>2</sup>. Details of the trough cleaning procedure can be found elsewhere.[22] The particles were first dispersed in the spreading solvent (mixture of water and isopropanol alcohol at a 1:1 vol. ratio) to a concentration of 0.5 wt%. 80  $\mu$ L of the 0.5 wt% particle suspension was spread carefully at the air-liquid interface ensuring that the suspension droplets were evenly distributed across the trough area. The deposited film was left undisturbed for 30 min to evaporate the spreading solvent. The surface pressure of the particle-laden interface was continuously measured as the trough area was reduced from 280 cm<sup>2</sup> to 20 cm<sup>2</sup> at a compression rate of 50 cm<sup>2</sup>/min. All measurements were repeated in triplicate and the results demonstrated good reproducibility (surface pressures at equivalent trough areas were within  $\pm 5\%$ ). Further details on the experimental setup and procedure can be found in our previous publication.[22]

2.2.2 Particle-laden interface structure The structure of the particle-laden interface was studied under several states of compression (low  $\rightarrow$  high surface pressures) using a Brewster Angle Microscope (BAM, Model EP3, Accurion GmbH, Germany) combined with a Langmuir trough.[36, 37] One advantage of combined Langmuir trough + BAM is that the structural changes associated with compression of the particle-laden interface can be measured in-situ without the need for ex-situ analysis of a Langmuir-Blodgett film.[38] In the current study, the BAM was equipped with light guides and a CCD camera used to image the particle-laden interface at  $\times 10$  magnification. Both the microscope and polarized light were initially aligned to the air-water Brewster angle,  $\theta_B \approx 53.22^\circ$ . With no p-polarized reflection (i.e. parallel light to the incident plane) from a clean air-water interface, reflected light was only measured following deposition of the particle-laden interface, with the reflected light intensity being a function of the particle surface coverage and film thickness.[39]

Three electrolyte concentrations (0.01 M, 0.1 M and 0.55 M Na<sub>2</sub>SO<sub>4</sub>) in the aqueous sub-phase were considered. The Brewster angle was calibrated for each electrolyte concentration (0.01 M  $\sim 53.23^\circ$ , 0.1 M  $\sim 53.27^\circ$  and 0.55 M  $\sim 53.45^\circ$ ) to achieve the best image quality (i.e. maximize the

contrast between the aqueous sub-phase and the particle layer). Following calibration, 80  $\mu\text{L}$  of the 0.5 wt% composite particle suspension was deposited at the air-aqueous interface in the spreading solvent. The deposited particle-laden interface was left undisturbed for 30 min prior to imaging. The particle-laden interfaces were compressed to several target surface pressures (0.5, 1, 2, 3, and 4 mN/m) from a maximum trough area of 320  $\text{cm}^2$ . The compressed particle-laden interfaces were allowed to relax for 1 min before imaging by BAM at constant pressure. The polarizer and analyzer were set to  $2^\circ$  and  $10^\circ$ , respectively. Images were collected using the EP3View2.x software (Accurion).

2.2.3 Interfacial shear rheology (ISR) The viscoelasticity of the particle-laden interfaces was studied under shear using an Interfacial Shear Rheometer (ISR400, Biolin Scientific,) combined with a KSV NIMA Langmuir trough (Biolin Scientific). The measurement region is enveloped by a pair of Helmholtz coils with one coil used to fix the orientation of the magnetic needle and the second coil producing a magnetic field gradient to drive the magnetic needle in motion. The needle had dimensions of radius ( $a$ ) = 0.27 mm, length ( $L$ ) = 55 mm and mass ( $m$ ) = 72 mg. To conduct the rheology measurements a hydrophobically modified magnetic needle was pinned at the air-aqueous interface and positioned within a roughened glass channel. A slight meniscus was generated by the glass channel to ensure that the magnetic needle was self-centred. An overhead CCD camera (Basler Electric Company) was focused on the needle such that one edge of the needle could be precisely tracked during oscillatory motion.[9] Edge detection was projected onto a linear image sensor with a 512-pixel photodiode array and pixel resolution of 3.58  $\mu\text{m}$ .

With the magnetic needle oscillating sinusoidally (induced by the Helmholtz coils), an amplitude ratio, AR, can be defined as the ratio of the amplitude of the rod displacement (strain,  $\gamma$ ) to the forcing amplitude (stress,  $\sigma$ ), with the strain and stress offset being the phase difference ( $\delta$ ). The dynamic surface modulus,  $G^*$ , which is given by  $G^*(\omega) = G'(\omega) + iG''(\omega)$ , can be determined directly from AR and  $\delta$  [40, 41]

$$G^*(\omega) = \frac{1}{AR} e^{i\delta} = G'(\omega) + iG''(\omega) \quad (1)$$

where  $G'$  and  $G''$  describe the storage and loss moduli of the interfacial film, respectively.

The operability of the ISR was recently considered and the limits to attain good-quality data discussed.[42] The needle inertia can be minimized by reducing the needle dimensions and mass.[43-45] While needle inertia becomes more prevalent for viscous or weakly elastic interfaces, for strongly elastic interfaces the contribution is lessened and the measured viscoelasticity becomes a true reflection of the interfacial rheology.[46] Another sensitivity of the ISR technique is to ensure that the surface stresses dominate the underlying sub-phase stresses. The requirement to decouple the surface stresses from the sub-phase bulk contribution can be assessed by the dimensionless Boussinesq number ( $Bo$ ), which is defined as the ratio of surface to bulk stresses.[46] For all particle-laden interfaces considered in the current study  $Bo \geq 20$ , indicating no requirement to decouple the sub-phase contribution. For this reason, all experimental data are presented without further processing.[19]

In a typical ISR measurement, 400  $\mu$ L of the aqueous sub-phase was first pipetted into the Langmuir trough. Prior to each measurement the needle was magnetized and positioned at the air-aqueous interface within the glass channel. The mobility of the magnetic needle was first calibrated on a particle-free interface such that the combined contribution from the sub-phase and needle inertia could be baseline subtracted from the measured response when oscillated in the presence of particles. 80  $\mu$ L of the 0.5 wt% particle suspension was then deposited at the air-aqueous interface following the film preparation procedure previously described. The particle-laden interface was left undisturbed for 30 min to evaporate the spreading solvent and then compressed at a rate of 10  $\text{cm}^2/\text{min}$  to several target surface pressures (0.5, 1, 2, 3, 4, 5 and 6  $\text{mN/m}$ ). To maintain a constant surface pressure the operational mode of the Langmuir trough was switched to pressure control mode during the rheological measurement.

For all particle-laden interfaces a dynamic strain sweep (amplitude sweep) was first conducted at a fixed frequency of 0.5 Hz (3.14 rad/s) to determine the linear viscoelastic region. Such measurements also provided guidance on the input voltages required to drive the magnetic needle

into oscillation with sufficient forward and backward motion. For example, for weak particle-laden interfaces (i.e. low surface pressures  $\sim 0.5$  mN/m) the optimal input voltage was in the range 0.05 to 0.8 V, while for more compressed interfaces (i.e. higher surface pressures  $\sim 3$  mN/m) the input voltage varied between 0.1 and 1.5 V. Details of the input voltages used in the current study are summarized in Table S1. To probe the time-dependent response of the particle-laden interfaces, frequency sweep measurements were conducted between 0.1 Hz (0.63 rad/s) and 5 Hz (31.40 rad/s), see Table S2 for experimental settings. All interfacial rheology tests were repeated three times with minimal experimental variability observed.

**2.3 Cryo-SEM** To prepare the particle-stabilized foams, 10 mL of a 1 wt% composite particle suspension prepared in either 0.1 M or 0.55 M  $\text{Na}_2\text{SO}_4$  was added to a 40 mL glass vial. The suspension was gently agitated for 5 min using a laboratory carousel before 1 min of vigorous handshaking to generate the foam. More details on the foaming procedure and foam characterization can be found in our recent publication.[22]

Cryo-SEM (Quorum Technologies, UK) was used to study the structure of the particle-laden interfaces surrounding air bubbles. Approximately 0.5 mL of the foam was pipetted onto a universal specimen shuttle (AL200077B) and plunged into liquid nitrogen at  $-196$  °C for 2 min.[47] The frozen sample was then transferred to a Quilo cryo preparation chamber ( $T = -175$  °C) under high vacuum ( $1 \times 10^{-7}$  mbar) using the system cryo transfer device. The preparation chamber with viewing window was used to remove excess ice by the twin fracturing manipulators. With the excess ice removed, the cryo samples were transferred onto a highly stable SEM cold stage for imaging at  $-150$  °C.

### 3. RESULTS AND DISCUSSION

**3.1  $\Pi$  – A isotherms and interfacial structure**  $\Pi$ -A isotherms of the deposited particle-laden interfaces are shown in Fig. 1. The effect of the sub-phase electrolyte concentration is evident, with the highest surface pressures measured for the highest electrolyte concentration. All particle-

laden interfaces exhibit gas (G), liquid (L), and solid (S) phases, showing an increase in the film collapse pressure with increasing  $\text{Na}_2\text{SO}_4$  concentration: 8 mN/m to 11 mN/m to 22 mN/m for 0.01 M to 0.1 M to 0.55 M  $\text{Na}_2\text{SO}_4$ , respectively.

The surface elasticity of the particle-laden interface upon compression was determined by,  $E_0 = -\frac{d\Pi}{d\ln A}$ , where  $A$  is the trough area and  $\Pi$  the surface pressure. The inset of Fig. 1 compares the surface elasticities for the three particle-laden interfaces (0.01 M, 0.1 M and 0.55 M  $\text{Na}_2\text{SO}_4$ ). An increase in the sub-phase electrolyte concentration leads to an increase in the surface elasticity of the particle-laden interface, thus confirming a stiffer particle network with greater resistance to compression. It should be noted that the observed differences in surface elasticities were unlikely to result from particle removal (detachment) from the air-aqueous interface. In our previous study, differences between consecutive compression and expansion cycles across equivalent trough areas (0.01 M  $\text{Na}_2\text{SO}_4$  particle-laden interface) were shown to be negligible when the surface pressure exceeded  $\sim 1.5$  mN/m, and hence the potential for particle removal under compression was thought to be insignificant. Also at higher electrolyte concentrations, particle retention at the air-aqueous interface would be further enhanced due to increased particle aggregation and a changing particle wettability which is governed by the polymer solvency in the electrolyte.[22] The increasing surface elasticity was thought to result from changes in the particle-particle interaction strength. Our previous study confirmed the aggregation of composite particles at a critical electrolyte concentration of 0.1 M  $\text{Na}_2\text{SO}_4$ . As measured by AFM, the particle-particle interaction was attractive between two composite particles in 0.1 M and 0.55 M  $\text{Na}_2\text{SO}_4$  with an apparent adhesion force measured during pull-off. For 0.01 M  $\text{Na}_2\text{SO}_4$ , the interaction was purely repulsive with no measurable adhesion.[22] The apparent softening of the particle-laden film at smaller trough areas was indicative of monolayer collapse as the surface pressure begins to saturate.

Interestingly, while the film collapse pressure was dependent on the electrolyte concentration, the compressional area at film collapse appears to be independent of the electrolyte concentration. This is clearly evident when comparing the surface elasticities of the three particle-laden interfaces, with the maximum surface elasticity corresponding to the collapse area (inset Fig. 1). For hard-

spheres this electrolyte independence does not hold true with the collapse area shown to increase with increasing electrolyte concentration.[48] This behaviour has been explained by the increased aggregation between particles, restricting particle mobility and producing a “rigid” space-spanning network at lower surface coverage. While increased particle aggregation at higher electrolyte concentration has also been shown in the current study (Fig. 2), this observed independence likely results from the deposited PVP layer around the nano silica particles. In our recent study we showed that two PVP-coated surfaces (silica) produce a lubrication effect when compressed together,[49] with the lubrication effect maintained, albeit to a reduced effect, when polymers are submerged in solutions of increasing electrolyte concentration.[50, 51] As such, the particle-particle contacts become mobile at a critical compressional stress, allowing the film to reorganize and densify to an almost self-similar structure before eventually collapsing (buckling or wrinkling).

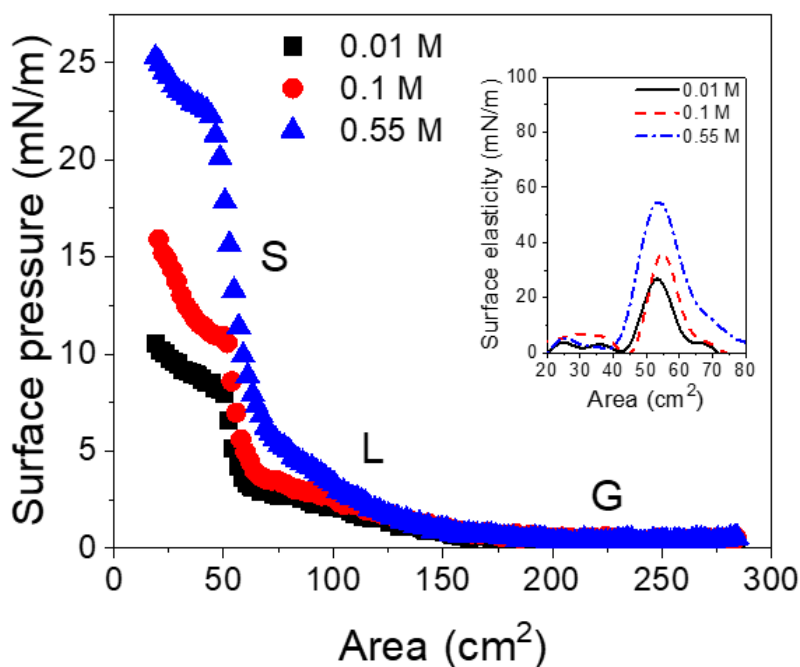


Figure 1.  $\Pi - A$  isotherms of composite particles deposited at the air-aqueous interface. The particle concentration and spreading volume remained fixed at 0.5 wt% and 80  $\mu\text{L}$ , respectively. The surface pressure was measured continuously at a compression rate of 50  $\text{cm}^2/\text{min}$ . The inset compares the surface elasticity ( $E_0 = -\frac{d\Pi}{d\ln A}$ ) of the three particle-laden interfaces as a function of surface area.

BAM was used to visualize the structures of the particle-laden interfaces at surface pressures  $\leq 5$  mN/m (Fig. 2). For 0.01 M  $\text{Na}_2\text{SO}_4$  and at the lowest surface pressure ( $\Gamma = 0.5$  mN/m), the BAM image was featureless and of uniformly dark grey color, hence no assessment of the particle-laden interface structure was made. However, as the particle-laden interface was compressed ( $\Gamma = 1, 2, 3$  mN/m) the BAM image became increasingly brighter as a result of increased densification of the particle network (increased surface coverage). The brightness of the image taken at the L-S phase boundary ( $\Gamma = 3$  mN/m) appeared to be uniform throughout, suggesting that the deposited particle-laden interface was homogenous, although intricate detail of the particle network structure was difficult to visualize since the particles remained dispersed at the lowest electrolyte concentration.

The onset of particle aggregation allowed for more interesting structural features to be identified. With consecutive increases in electrolyte concentration it was readily shown that the particle-laden interface ( $\Gamma = 0.5$  and 1 mN/m) became less homogenous with dark (voids) and bright (particle aggregates/clusters) spots being clearly observed. At the highest electrolyte concentration (0.55 M  $\text{Na}_2\text{SO}_4$ ) the voids in the particle-laden interface were significant, with the void size observed to decrease with increasing surface pressure.

As a function of the electrolyte concentration and surface pressure, the grey-scale contrast between the particle network and aqueous sub-phase can be used to provide an approximation of the particle surface coverage at the air-water interface. BAM images were processed using ImageJ software with a band pass filter used to correct for the varying illumination prior to thresholding.[52] While different approaches were considered to determine the most appropriate threshold value for distinguishing between the two phases (voids and particle aggregates), visual comparison of the BAM and grey-scaled images was found to be the most reliable. A sensitivity assessment on the chosen threshold value showed that a  $\pm 5\%$  change in the threshold value would result in a 4.5 – 6 % variability in the quoted apparent particle surface coverage. Assessment of the apparent particle surface coverage was made by analysing three images (dimensions –  $390 \times 490 \mu\text{m}$ ) along

the centreline of the trough from the barrier edge to the mid-point between the two Langmuir trough barriers.

Fig. 3 compares the apparent particle surface coverages for the 0.1 M and 0.55 M  $\text{Na}_2\text{SO}_4$  particle-laden interfaces as a function of the surface pressure. Intuitively, the particle network compresses as the surface pressure increases, hence the particle surface coverage increases. The apparent particle surface coverage of the 0.55 M  $\text{Na}_2\text{SO}_4$  particle-laden interface was consistently below that of the 0.1 M particle-laden interface at equivalent surface pressures. As is clearly shown, the lower particle surface coverage results from a higher degree of particle aggregation which has been reported in our previous study.[22] For 0.1 M  $\text{Na}_2\text{SO}_4$ , the apparent particle surface coverage increased from  $\sim 70\%$  to almost complete coverage ( $\sim 99\%$ ), while the average void size reduced from approximately  $4\ \mu\text{m}^2$  ( $\sim 4.1\ \mu\text{m}^2$ ) to less than  $1\ \mu\text{m}^2$  ( $\sim 0.7\ \mu\text{m}^2$ ) as the surface pressure was increased from 0.5 mN/m to 4 mN/m. At the highest electrolyte concentration (0.55 M  $\text{Na}_2\text{SO}_4$ ), the apparent particle surface coverage increased from  $\sim 27\%$  to  $\sim 80\%$ , while the average void size reduced from greater than  $1000\ \mu\text{m}^2$  ( $\sim 1135\ \mu\text{m}^2$ ) to less than  $10\ \mu\text{m}^2$  ( $\sim 7\ \mu\text{m}^2$ ) across the same range of surface pressures.

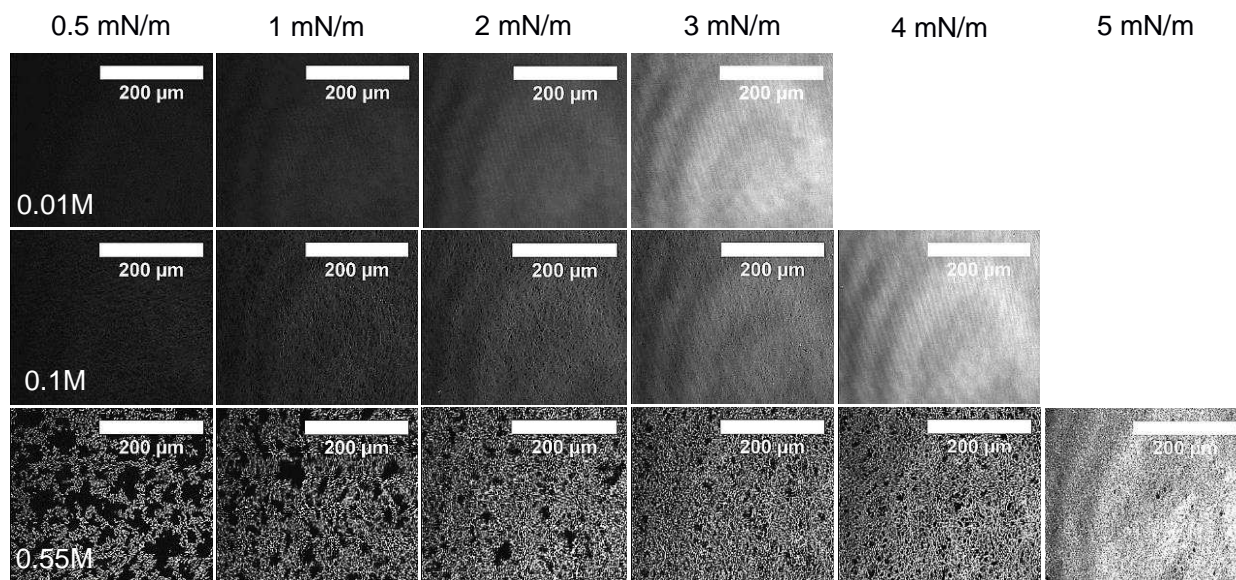


Figure 2. BAM images of composite particles deposited at the air-water interface as a function of the sub-phase electrolyte concentration (as labelled 0.01 M, 0.1 M, and 0.55 M  $\text{Na}_2\text{SO}_4$ ) and

surface pressures. Higher electrolyte concentrations increased voidage in the particle-laden films, which can be attributed to aggregation of the composite particles. Surface pressure driven densification of the particle-laden films was qualitatively verified by the reduced voidage and increased brightness of the BAM images.

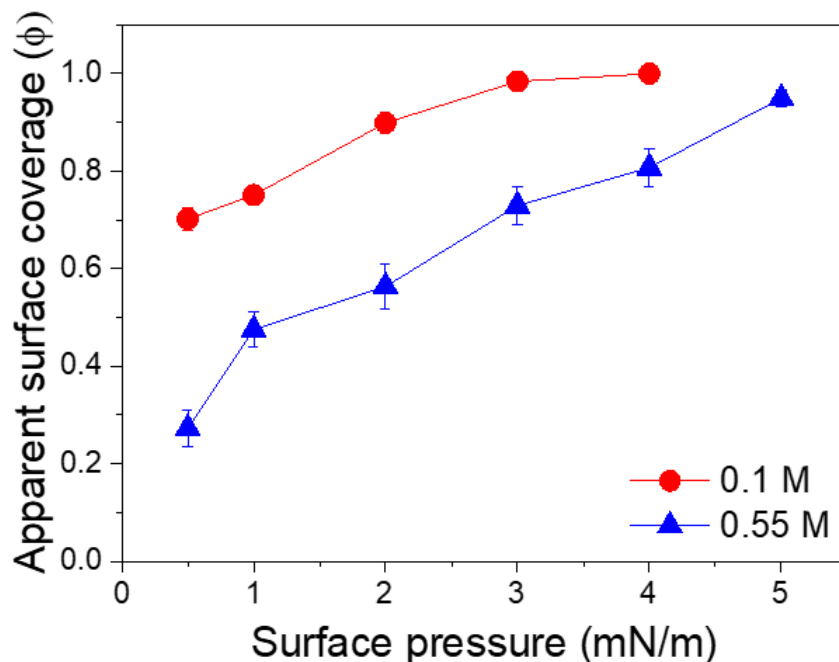


Figure 3. Apparent particle surface coverage ( $\phi$ ) of 0.1 M and 0.55 M  $\text{Na}_2\text{SO}_4$  particle-laden interfaces. BAM images were processed using ImageJ, first correcting for varying illumination using a band pass filter and thresholded to differentiate between the sub-phase and particle network.

**3.2 Interfacial rheology** The shear rheology of the particle-laden interface was studied using the ISR needle rheometer, with the elastic ( $G'$ ) and viscous ( $G''$ ) contributions measured as a function of the sub-phase electrolyte concentration and surface pressure. Having attained the target surface pressure, the Langmuir trough barriers were operated in feedback mode to ensure the surface pressure remained constant during the rheology measurement. To assess the mechanical properties of the particle-laden interfaces, the magnetic needle was oscillated at an amplitude within the linear viscoelastic region and at a constant frequency of  $F = 0.5$  Hz (3.14 rad/s).

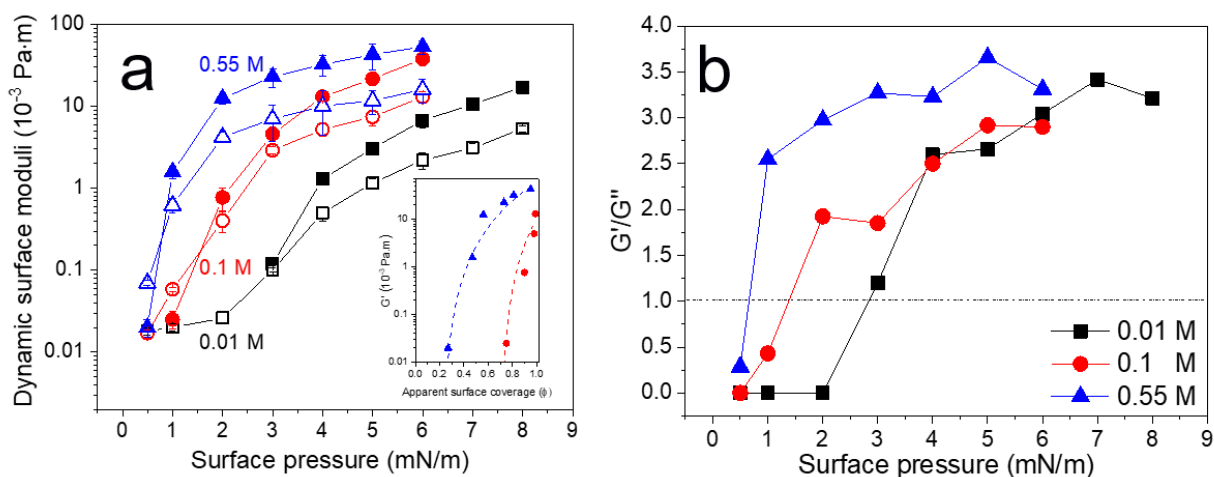


Figure 4. a) Dynamic surface shear moduli ( $G'$  – closed symbols and  $G''$  – open symbols) and b)  $G'/G''$  ratio of the particle-laden interfaces as a function of the sub-phase electrolyte concentration and surface pressure. The magnetic needle was oscillated at a constant frequency ( $\omega = 3.14$  rad/s) and amplitude in the linear viscoelastic region. The dynamic surface shear moduli were determined using Eq. 1. Inset a) shows the dependence of  $G'$  on the apparent surface coverage ( $\phi$ ). The dash lines are given by  $G' = A(\phi - \phi_c)^3$ , where  $A$  is an adjustable parameter and  $\phi_c$  is the critical surface coverage taken to be 0.22 and 0.71 for 0.55 M and 0.1 M  $\text{Na}_2\text{SO}_4$ , respectively, in good agreement with the BAM assessment.

Fig. 4a compares the dynamic surface shear moduli of the three particle-laden interfaces under increased compression. The viscoelastic response to the compressional force was consistent for all three particle-laden interfaces, and resembled the typical rheological profile of an aging interface, for example oil-water interfaces stabilized by asphaltenes which exhibit a time-dependent viscous-to-elastic transition as the asphaltenes accumulate (increased surface coverage) and reorganize at the oil-water interface. [53] At the lowest surface pressure ( $\Pi = 0.5$  mN/m), all three particle-laden interfaces were viscous dominant and can be considered liquid-like. However, as the imposed surface pressure increased, the contribution of the two viscoelastic moduli increased at different rates, eventually attaining an elastically dominant (i.e. solid-like) interface. It is

interesting to note the critical surface pressure to promote this transition ( $G' = G''$ ) was shown to be a function of the sub-phase electrolyte concentration (Fig. 4b).

At the lowest electrolyte concentration (0.01 M Na<sub>2</sub>SO<sub>4</sub>) and low surface pressures ( $\Pi < 3$  mN/m), the particle-laden interface was purely viscous with an immeasurably small shear elasticity. At these surface pressures the particle-laden interface was in the L-phase, and due to the repulsive interaction[22] the particles were freely mobile under the applied shear. The viscous and elastic contributions measured at  $\Pi = 3$  mN/m were almost equivalent, while at higher surface pressures in the S-phase ( $\Pi = 3 - 8$  mN/m) the viscoelastic ratio ( $G'/G''$ ) increased sharply up to  $\Pi = 4$  mN/m, indicating the strongly elastic nature of the compressed particle-laden interface. Eventually a maximum viscoelastic ratio of  $\sim 3.2$  was reached as the particle-laden interface approached the collapse pressure. Similar trends in the surface pressure dependent viscoelastic response were observed when increasing the electrolyte concentration. However, the surface pressure to satisfy the condition  $G' = G''$  was observed to decrease (Fig. 4b), with the 0.55 M Na<sub>2</sub>SO<sub>4</sub> particle-laden interface being strongly elastic when  $\Pi = 1$  mN/m, a condition which can be considered well below the L- to S-phase transition pressure (Fig. 1). The increased elasticity at low surface pressures can be attributed to the higher degree of particle aggregation which promotes the formation of a contiguous, space spanning network when the apparent particle surface coverage is low.

As shown in Fig. 4a, the magnitude of the viscoelastic response (when compared at equivalent surface pressures) increased with increasing sub-phase electrolyte concentration. This type of response is indicative of the structural differences, most likely governed by the particle coverage and the particle-particle interaction strength (i.e. the modulus of the individual composite particles). The relative contribution from the two governing parameters is not readily apparent, although the particle-particle interaction strength which is controlled by the sub-phase electrolyte concentration is shown to have a dramatic influence on the magnitude of the viscoelastic moduli, in good agreement with previous observations.[54] However, while the magnitude of the viscoelastic responses were different, it is interesting to note that the viscoelastic ratio for all three systems appeared to plateau towards  $G'/G'' \sim 3.0$  (Fig. 4b), underlining that the shear viscoelastic response becomes independent of the surface pressure when the particles are in a close-packed lattice above

a critical surface coverage,  $\phi_c$ , i.e. approaching a jammed state.[55] This characteristic response appears to indicate once again that the particle networks, independent of the sub-phase electrolyte concentration, become self-similar at high surface pressures when the axial compression dictates the structure forming parameters. This self-similarity at high surface pressures complements the observed independence of the critical compression area at film collapse as a function of the electrolyte concentration (Fig. 1). Fig. 1 also confirms that the viscoelastic ratios plateaued within the S-phase for 0.01 M and 0.1 M  $\text{Na}_2\text{SO}_4$  particle-laden interfaces, while it was observed to be in the L-phase at the highest electrolyte concentration.

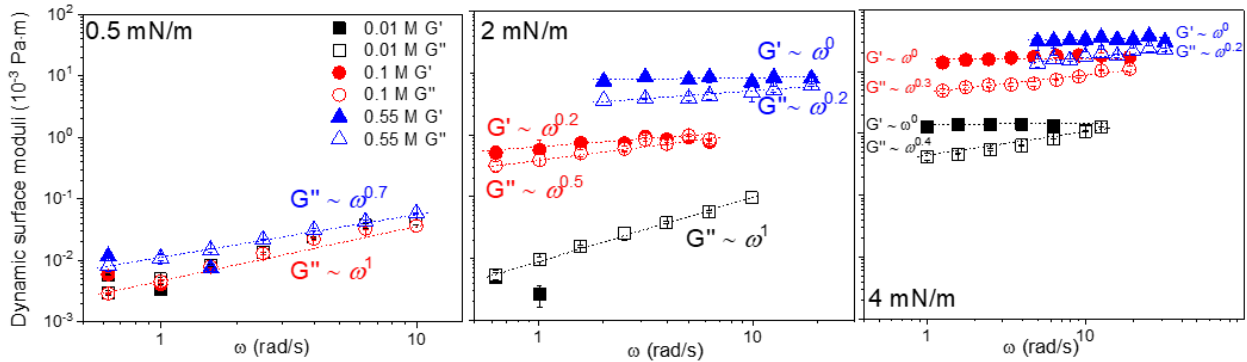


Figure 5. Frequency dependent dynamic surface moduli ( $G'$  – closed symbols and  $G''$  – open symbols) of the particle-laden interfaces as a function of the sub-phase electrolyte concentration (symbols shown inset) and surface pressure (as labelled). The power-law scaling confirms the transition from liquid- to solid-like behaviour with increasing surface pressure and sub-phase electrolyte concentration.

To better understand the time-dependent dynamics of the particle-laden interfaces, frequency-sweep measurements were performed in the linear viscoelastic regime. Fig. 5 shows the dynamic surface moduli measured as a function of the oscillation frequency. At low surface pressure ( $\Pi = 0.5 \text{ mN/m}$ ), the response of all three particle-laden interfaces was characteristically viscous, varying with  $\omega^{-1}$  and independent of the sub-phase electrolyte concentrations. At higher frequencies,  $G'$  was immeasurable as the phase difference between the stress and strain approached  $90^\circ$ . [40]

At intermediate surface pressures ( $\Pi = 2 \text{ mN/m}$ ), the 0.01 M  $\text{Na}_2\text{SO}_4$  particle-laden interface remained viscous dominant, while a viscoelastic transition was measured for the 0.1 M and 0.55 M  $\text{Na}_2\text{SO}_4$  particle-laden interfaces. The  $G'$  and  $G''$  dependence on the oscillation frequency decreased with increasing electrolyte concentration. For example, the  $G'$  response of the 0.55 M  $\text{Na}_2\text{SO}_4$  particle-laden interface showed a frequency independent plateau, signifying the onset of the glassy state when the dynamics of the system become frozen.[56] At the highest surface pressure all particle-laden interfaces exhibited a frequency independent plateau of  $G'$ , which was expected as the apparent particle surface coverage approached 100%, although the plateau can be achieved at lower apparent particle surface coverages when the attractive potential between the composite particles is strong, for example 0.55 M  $\text{Na}_2\text{SO}_4$ . While no definitive crossover in the viscoelastic moduli was measured in the frequency range, the dependence of  $G''$  on  $\omega$  ( $\Pi = 4 \text{ mN/m}$ ) suggests that the high frequency response is influenced by the viscous forces,[57] i.e. the sub-phase fluid viscosity and confined polymer layers.

**3.3 Yield point determination** In the solid-like state ( $G' > G''$ ) particle-laden interfaces exhibit a critical yield which must be exceeded for the particles (particle domains) to flow. Dynamic strain-amplitude sweeps at a constant frequency ( $\omega = 3.14 \text{ rad/s}$ ) were performed to measure the yield modulus as a function of the sub-phase electrolyte concentration and surface pressure. Fig. S2 shows the characteristic responses of the particle-laden interfaces to the increased strain. At low amplitude (strain) the viscoelastic moduli were independent of the applied deformation, signifying the characteristic linear viscoelastic response. With increasing strain, both moduli decreased as the mechanical strength of the particle-laden interface was weakened. A critical strain was attained when  $G' = G''$  and the particle-laden interface had yielded. Beyond yielding the film response to deformation (strain) was dominated by viscous forces. In the nonlinear regime the ratio of slopes of  $G'$  and  $G''$  was  $\sim 2$  (Fig. S2), in good agreement with previously reported values for yielding interfaces.[27]

Fig. 6a shows the dependence of the particle-laden interface yield modulus on the sub-phase electrolyte concentration and surface pressure. For all systems the yield modulus increased with surface pressure and increasing electrolyte concentration (yield modulus at equivalent surface

pressures), the latter consistent with the increased particle aggregation in 0.1 M and 0.55 M Na<sub>2</sub>SO<sub>4</sub> electrolyte. At the lowest electrolyte concentration (0.01 M) the particle-laden interface yield modulus was only measured in the S-phase region, i.e. under high compression. The increase in yield modulus was moderate and almost linear with increasing surface pressure. For the intermediate electrolyte concentration (0.1 M) the yield modulus was measured in both the L- and S-phases (slightly beyond the transition pressure). The linear dependence of the yield modulus on surface pressure was once again observed up to  $\Pi = 4 \text{ mN/m}$ , beyond which the yield modulus became almost independent of the surface pressure when in the S-phase region. The reduced dependency of yield modulus on surface pressure in the S-phase is in good agreement with the 0.01 M Na<sub>2</sub>SO<sub>4</sub> system. At the highest electrolyte concentration (0.55 M) the yield modulus was measured only in the L-phase region (L-to-S phase transition  $\Pi \sim 6 \text{ mN/m}$ ). While there is slight fluctuation in the data, the trend is approximately linear (yield modulus vs. surface pressure) and in good agreement with the L-phase characteristic response.

Fig. 6b compares the apparent yield strain for all systems. The yield strain reflects the amount of interfacial deformation required to yield the particle-laden interface, with an interface of low yield strain and high yield stress often described as brittle.[46] While the apparent yield strain remains relatively low for the two cases where attraction between the composite particles is prevalent, the apparent yield strain of the 0.01 M Na<sub>2</sub>SO<sub>4</sub> particle-laden interface appears more sensitive to the surface pressure, with the yielding properties characterized by ductile and brittle responses at low and high surface pressures, respectively.

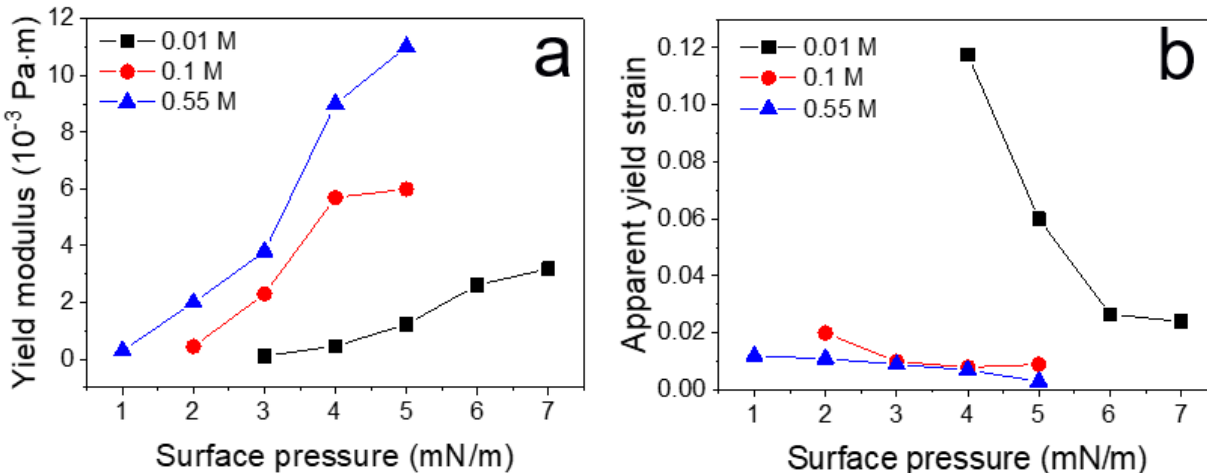


Figure 6. a) Yield modulus ( $G' = G''$ ) and b) apparent yield strain of particle-laden interfaces as a function of the sub-phase electrolyte concentration and surface pressure. The apparent yield strain was determined based on the condition  $G' = G''$  as shown in Fig. S2.

**3.4 Particle-stabilized bubbles** A unique feature of the ISR is the ability to accurately adjust the surface pressure applied to a particle-laden interface and measure the pressure-dependent interfacial rheology. Correlating the rheology and film structure can then provide new insights to the likely rheology of bubble stabilizing particle networks. Extrapolating the rheology measured at a planar interface to that of a curved interface is only sensible if the two radii of curvature (particle and bubble) are sufficiently contrasting such that the particle ‘sees’ the interface as being effectively planar.

Particle-stabilized foams were imaged using cryo-SEM such that the structure of the particle-laden interface surrounding an air bubble could be elucidated. Fig. 7 shows low and high magnification images of single bubbles isolated in foams prepared with composite particles dispersed in 0.1 M (Fig. 7a) and 0.55 M (Fig. 7b)  $\text{Na}_2\text{SO}_4$  electrolyte. The typical bubble size ( $D_b$ ) following foaming was greater than 100  $\mu\text{m}$  and the hydrodynamic diameter ( $D_h$ ) of the composite particle was  $\sim 52$  nm, thus the  $D_b/D_h$  ratio was of the order of  $\sim 10^3$ . At this ratio simple geometric arguments confirmed the reliability of evaluating the likely rheology of the bubble stabilizing particle network from the rheology measured at a planar interface (i.e. ISR).

Firstly on assessment of the cryo-SEMs, the structures of the bubble stabilizing particle networks showed good similarity to those measured by BAM (Fig. 2). At the highest electrolyte concentration (0.55 M Na<sub>2</sub>SO<sub>4</sub>) the structure of the particle-laden interface was heterogeneous with fractures sparingly distributed throughout the film (Fig. 7b), which contrasted the homogenous and densely packed particle-laden interface observed for the intermediate electrolyte (0.1 M Na<sub>2</sub>SO<sub>4</sub>) foam (Fig. 7a). Those structures visually compared to the BAM images obtained at the higher surface pressures. Using the previously described thresholding method we determine that the apparent particle surface coverage stabilizing air bubbles in foams was approximately 100% and 95% for 0.1 M and 0.55 M Na<sub>2</sub>SO<sub>4</sub> foams, respectively. Referring to Fig. 3, those apparent particle surface coverages indicate that the surface pressure of the bubble stabilizing particle networks was  $\Pi = 4$  mN/m (0.1 M Na<sub>2</sub>SO<sub>4</sub>) and  $\Pi \sim 5$  mN/m (0.55 M Na<sub>2</sub>SO<sub>4</sub>). Quite interestingly both surface pressures correspond to a particle-laden interface at the L-S phase transition, and an interfacial shear rheology which is strongly elastic.

It should be acknowledged that while the two methods of forming particle-stabilized interfaces differ (i) particle adsorption in foaming and (ii) particle deposition via spreading at an air-water interface, the resulting structures of the particle networks are remarkably similar for methods (i) and (ii). This is not unexpected since the method to bring particles close to an interface does not influence the final position which is governed by the pinning of the contact line on the surface of the particle.[35, 58, 59]

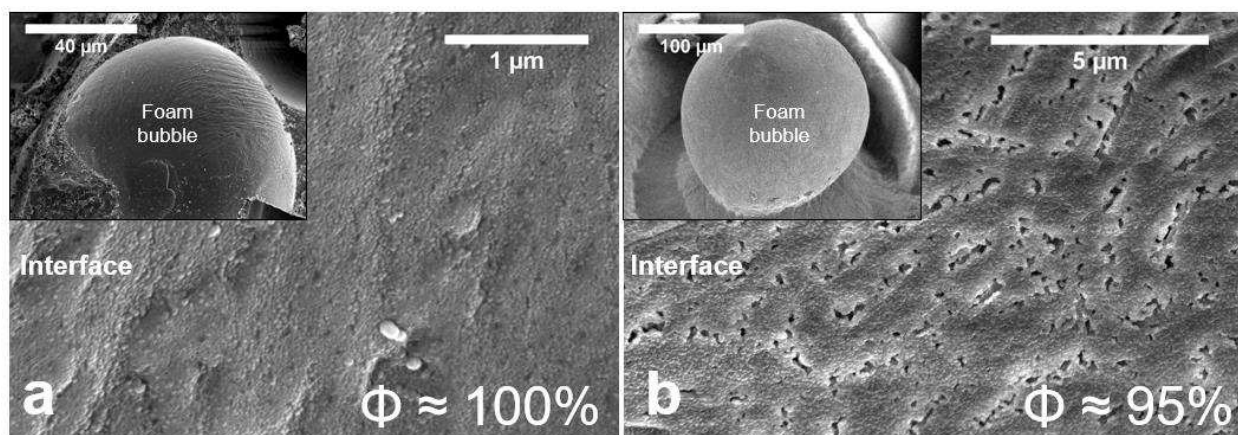


Figure 7. Particle-laden interfaces surrounding air bubbles: a) 0.1 M Na<sub>2</sub>SO<sub>4</sub> foam, and b) 0.55 M Na<sub>2</sub>SO<sub>4</sub> foam. The individual bubble is shown in the inset of the higher magnification interfacial image.

#### 4. CONCLUSION

The current study considered the influence of sub-phase electrolyte concentration and surface pressure on the rheology of composite particle-laden interfaces. Silica nanoparticles stabilized by PVP formed highly dispersed and homogenous particle-laden interfaces, which evolved into aggregated, space spanning networks when the electrolyte concentration was increased. Under axial compression all particle-laden interfaces underwent gas-liquid-solid phase transitions before collapse of the particle network structure at high surface pressures.

The surface shear moduli of all particle-laden interfaces exhibited a liquid- to solid-like transition with increasing surface pressure, and the critical surface pressure at transition was shown to be a function of the sub-phase electrolyte concentration. While the particle-particle interaction strength predominantly affected the magnitude of the viscoelastic moduli, at higher surface pressures the viscoelastic ratio ( $G'/G''$ ) became almost independent of the sub-phase electrolyte concentration, possibly indicating self-similarity of the particle networks once the axial compression dictates the structure forming parameters. Such behavior in different electrolyte environments was thought to relate to the lubricating potential of the particle polymer-shell, a unique feature exhibited by the composite particles.

The use of composite nanoparticles as the stabilizing species provided insight to the likely rheology of the bubble stabilizing particle network. The particle network structure surrounding an air bubble and deposited at a planar interface were correlated using cryo-SEM and BAM images. At intermediate and high electrolyte concentrations it would appear that the structure of the particle-laden interface (surrounding an air bubble) was close-packed, with a surface pressure at the L-S phase transition boundary. At this condition the shear rheology of the particle-laden films was strongly elastic, although the particle-laden interfaces exhibited a low yielding strain due to their brittleness, possibly an influence of the contact lubricating effect.

For composite particles the interfacial rheology becomes a function of the localized mechanical response of the soft particle-shell and rigid particle-core. While the relative contributions from the core and shell are not readily discernible in the current study, this is part of our ongoing effort. Due to their hybrid structure, composite particles are increasingly more interesting with an ability to finely adjust their mechanical response, and hence find greater application in the formulation of novel soft matter materials.

## **ASSOCIATED CONTENT**

### **Supporting Information**

TEM images of the PVP-coated silica nanoparticles clearly showing the core-shell structure of the composite particles (Fig. S1); Strain sweep settings for the ISR measurements (Table S1); Frequency sweep settings for the ISR measurements (Table S2); Dynamic strain sweep of an elastically dominant particle-laden interface (0.01 M Na<sub>2</sub>SO<sub>4</sub>). At small strains the dynamic shear moduli are independent of strain before the particle-laden interface yields ( $G' = G''$ ). The yielding dynamics are described by  $G' \sim \gamma_0^{-\nu'}$  and  $G'' \sim \gamma_0^{-\nu''}$  where  $\nu' \sim 2\nu''$  (Fig. S2).

### **Corresponding Author**

D.H. – Email: [D.Harbottle@leeds.ac.uk](mailto:D.Harbottle@leeds.ac.uk), Tel: +44 (0)113 343 4154

## **ACKNOWLEDGMENTS**

K.Y. thanks the China Scholarship Council (Scholarship No. 201406450027) and the Worldwide Universities Network (Researcher Mobility Award, University of Leeds) for supporting this research. The authors would like to acknowledge the experimental assistance of Mrs. Ni Yang (NINT, University of Alberta, Canada) who provided guidance on using the ISR, along with Mr. Robert Morrison and Ms. Heather Dyson (Quorum Technologies, UK), and Dr. Nicole Hondow (University of Leeds) who provided access and support on using state-of-the-art cryo-SEM facilities.

## References

- [1] B.P. Binks, R. Murakami, Phase inversion of particle-stabilized materials from foams to dry water, *Nat Mater* 5(11) (2006) 865-869.
- [2] J.P. Hitchcock, A.L. Tasker, E.A. Baxter, S. Biggs, O.J. Cayre, Long-Term Retention of Small, Volatile Molecular Species within Metallic Microcapsules, *Acs Appl Mater Inter* 7(27) (2015) 14808-14815.
- [3] E. Dickinson, Biopolymer-based particles as stabilizing agents for emulsions and foams, *Food Hydrocolloid* 68 (2017) 219-231.
- [4] M. Grauzinyte, J. Forth, K.A. Rumble, P.S. Clegg, Particle-Stabilized Water Droplets that Sprout Millimeter-Scale Tubes, *Angew Chem Int Edit* 54(5) (2015) 1456-1460.
- [5] V. Garbin, Colloidal particles: Surfactants with a difference, *Phys Today* 66(10) (2013) 68-69.
- [6] V. Lotito, T. Zambelli, Approaches to self-assembly of colloidal monolayers: A guide for nanotechnologists, *Adv Colloid Interfac* 246 (2017) 217-274.
- [7] B.P. Binks, Particles as surfactants - similarities and differences, *Curr Opin Colloid In* 7(1-2) (2002) 21-41.
- [8] E. Dickinson, Food emulsions and foams: Stabilization by particles, *Curr Opin Colloid In* 15(1-2) (2010) 40-49.
- [9] P. Cicuta, E.J. Stancik, G.G. Fuller, Shearing or compressing a soft glass in 2D: Time-concentration superposition, *Phys Rev Lett* 90(23) (2003).
- [10] S. Reynaert, P. Moldenaers, J. Vermant, Interfacial rheology of stable and weakly aggregated two-dimensional suspensions, *Phys Chem Chem Phys* 9(48) (2007) 6463-6475.
- [11] T.S. Horozov, R. Aveyard, J.H. Clint, B. Neumann, Particle zips: Vertical emulsion films with particle monolayers at their surfaces, *Langmuir* 21(6) (2005) 2330-2341.
- [12] V. Garbin, J.C. Crocker, K.J. Stebe, Nanoparticles at fluid interfaces: Exploiting capping ligands to control adsorption, stability and dynamics, *J Colloid Interf Sci* 387 (2012) 1-11.
- [13] T.S. Horozov, B.P. Binks, Particle-stabilized emulsions: A bilayer or a bridging monolayer?, *Angew Chem Int Edit* 45(5) (2006) 773-776.
- [14] E. Jarrett, P.M. Ireland, G.B. Webber, E.J. Wanless, Particle-liquid structures formed by electric fields, *Powder Technol* 297 (2016) 1-7.
- [15] A. Maestro, E. Guzman, F. Ortega, R.G. Rubio, Contact angle of micro- and nanoparticles at fluid interfaces, *Curr Opin Colloid In* 19(4) (2014) 355-367.
- [16] A. Maestro, L.J. Bonales, H. Ritacco, R.G. Rubio, F. Ortega, Effect of the spreading solvent on the three-phase contact angle of microparticles attached at fluid interfaces, *Phys Chem Chem Phys* 12(42) (2010) 14115-14120.
- [17] K.D. Danov, P.A. Kralchevsky, B.N. Naydenov, G. Brenn, Interactions between particles with an undulated contact line at a fluid interface: Capillary multipoles of arbitrary order, *J Colloid Interf Sci* 287(1) (2005) 121-134.
- [18] T.S. Horozov, R. Aveyard, B.P. Binks, J.H. Clint, Structure and stability of silica particle monolayers at horizontal and vertical octane-water interfaces, *Langmuir* 21(16) (2005) 7405-7412.
- [19] H. Zhang, K. Yu, O.J. Cayre, D. Harbottle, Interfacial Particle Dynamics: One and Two Step Yielding in Colloidal Glass, *Langmuir* 32(50) (2016) 13472-13481.
- [20] P.H.F. Hansen, L. Bergstrom, Perikinetic aggregation of alkoxyated silica particles in two dimensions, *J Colloid Interf Sci* 218(1) (1999) 77-87.

- [21] L.J. Bonales, J.E.F. Rubio, H. Ritacco, C. Vega, R.G. Rubio, F. Ortega, Freezing Transition and Interaction Potential in Monolayers of Microparticles at Fluid Interfaces, *Langmuir* 27(7) (2011) 3391-3400.
- [22] K. Yu, H. Zhang, C. Hodges, S. Biggs, Z. Xu, O.J. Cayre, D. Harbottle, Foaming Behavior of Polymer-Coated Colloids: The Need for Thick Liquid Films, *Langmuir* 33(26) (2017) 6528-6539.
- [23] D. Harbottle, Q. Chen, K. Moorthy, L.X. Wang, S.M. Xu, Q.X. Liu, J. Sjoblom, Z.H. Xu, Problematic Stabilizing Films in Petroleum Emulsions: Shear Rheological Response of Viscoelastic Asphaltene Films and the Effect on Drop Coalescence, *Langmuir* 30(23) (2014) 6730-6738.
- [24] A.J. Morse, S.Y. Tan, E.C. Giakoumatos, G.B. Webber, S.P. Armes, S. Ata, E.J. Wanless, Arrested coalescence behaviour of giant Pickering droplets and colloidosomes stabilised by poly(tert-butylaminoethyl methacrylate) latexes, *Soft Matter* 10(31) (2014) 5669-5681.
- [25] E.J. Stancik, A.L. Hawkinson, J. Vermant, G.G. Fuller, Dynamic transitions and oscillatory melting of a two-dimensional crystal subjected to shear flow, *J Rheol* 48(1) (2004) 159-173.
- [26] D.E. Tambe, M.M. Sharma, The Effect of Colloidal Particles on Fluid-Fluid Interfacial Properties and Emulsion Stability, *Adv Colloid Interfac* 52 (1994) 1-63.
- [27] D.Y. Zang, D. Langevin, B.P. Binks, B.B. Wei, Shearing particle monolayers: Strain-rate frequency superposition, *Phys Rev E* 81(1) (2010).
- [28] P.J. Beltramo, M. Gupta, A. Aliche, I. Liascukiene, D.Z. Gunes, C.N. Baroud, J. Vermant, Arresting dissolution by interfacial rheology design, *P Natl Acad Sci USA* 114(39) (2017) 10373-10378.
- [29] M. Safouane, D. Langevin, B.P. Binks, Effect of particle hydrophobicity on the properties of silica particle layers at the air-water interface, *Langmuir* 23(23) (2007) 11546-11553.
- [30] R. Van Hooghten, V.E. Blair, A. Vananroye, A.B. Schofield, J. Vermant, J.H.J. Thijssen, Interfacial Rheology of Sterically Stabilized Colloids at Liquid Interfaces and Its Effect on the Stability of Pickering Emulsions, *Langmuir* 33(17) (2017) 4107-4118.
- [31] F. Ravera, E. Santini, G. Loglio, M. Ferrari, L. Liggieri, Effect of nanoparticles on the interfacial properties of liquid/liquid and liquid/air surface layers, *J Phys Chem B* 110(39) (2006) 19543-19551.
- [32] L. Liggieri, E. Santini, E. Guzman, A. Maestro, F. Ravera, Wide-frequency dilational rheology investigation of mixed silica nanoparticle-CTAB interfacial layers, *Soft Matter* 7(17) (2011) 7699-7709.
- [33] A. Maestro, E. Santini, D. Zabiegaj, S. Llamas, F. Ravera, L. Liggieri, F. Ortega, R.G. Rubio, E. Guzman, Particle and Particle-Surfactant Mixtures at Fluid Interfaces: Assembly, Morphology, and Rheological Description, *Adv Cond Matter Phys* (2015).
- [34] A.J. Mendoza, E. Guzman, F. Martinez-Pedrero, H. Ritacco, R.G. Rubio, F. Ortega, V.M. Starov, R. Miller, Particle laden fluid interfaces: Dynamics and interfacial rheology, *Adv Colloid Interfac* 206 (2014) 303-319.
- [35] D.Y. Zang, E. Rio, D. Langevin, B. Wei, B.P. Binks, Viscoelastic properties of silica nanoparticle monolayers at the air-water interface, *Eur Phys J E* 31(2) (2010) 125-134.
- [36] D.Y. Zang, A. Stocco, D. Langevin, B.B. Wei, B.P. Binks, An ellipsometry study of silica nanoparticle layers at the water surface, *Phys Chem Chem Phys* 11(41) (2009) 9522-9529.
- [37] A. Stocco, E. Rio, B.P. Binks, D. Langevin, Aqueous foams stabilized solely by particles, *Soft Matter* 7(4) (2011) 1260-1267.

- [38] E. Pensini, D. Harbottle, F. Yang, P. Tchoukov, Z.F. Li, I. Kailey, J. Behles, J. Masliyah, Z.H. Xu, Demulsification Mechanism of Asphaltene-Stabilized Water-in-Oil Emulsions by a Polymeric Ethylene Oxide Propylene Oxide Demulsifier, *Energ Fuel* 28(11) (2014) 6760-6771.
- [39] R. Xu, E. Dickinson, B.S. Murray, Morphological changes in adsorbed protein films at the air-water interface subjected to large area variations, as observed by Brewster angle microscopy, *Langmuir* 23(9) (2007) 5005-5013.
- [40] C.F. Brooks, G.G. Fuller, C.W. Frank, C.R. Robertson, An interfacial stress rheometer to study rheological transitions in monolayers at the air-water interface, *Langmuir* 15(7) (1999) 2450-2459.
- [41] C.A. Naumann, C.F. Brooks, G.G. Fuller, W. Knoll, C.W. Frank, Viscoelastic properties of lipopolymers at the air-water interface: A combined interfacial stress rheometer and film balance study, *Langmuir* 15(22) (1999) 7752-7761.
- [42] T. Verwijlen, P. Moldenaers, H.A. Stone, J. Vermant, Study of the Flow Field in the Magnetic Rod Interfacial Stress Rheometer, *Langmuir* 27(15) (2011) 9345-9358.
- [43] J. Tajuelo, J.M. Pastor, F. Martinez-Pedrero, M. Vazquez, F. Ortega, R.G. Rubio, M.A. Rubio, Magnetic Microwire Probes for the Magnetic Rod Interfacial Stress Rheometer, *Langmuir* 31(4) (2015) 1410-1420.
- [44] J. Tajuelo, J.M. Pastor, M.A. Rubio, A magnetic rod interfacial shear rheometer driven by a mobile magnetic trap, *J Rheol* 60(6) (2016) 1095-1113.
- [45] J. Tajueo, E. Guzman, F. Ortega, R.G. Rubio, M.A. Rubio, Phase Diagram of Fatty Acid Langmuir Monolayers from Rheological Measurements, *Langmuir* 33(17) (2017) 4280-4290.
- [46] D. Truzzolillo, H. Sharaf, U. Jonas, B. Loppinet, D. Vlassopoulos, Tuning the Structure and Rheology of Polystyrene Particles at the Air-Water Interface by Varying the pH, *Langmuir* 32(27) (2016) 6956-6966.
- [47] B.P. Binks, M. Kirkland, J.A. Rodrigues, Origin of stabilisation of aqueous foams in nanoparticle-surfactant mixtures, *Soft Matter* 4(12) (2008) 2373-2382.
- [48] S. Razavi, K.D. Cao, B.H. Lin, K.Y.C. Lee, R.S. Tu, I. Kretzschmar, Collapse of Particle-Laden Interfaces under Compression: Buckling vs Particle Expulsion, *Langmuir* 31(28) (2015) 7764-7775.
- [49] K. Yu, C. Hodges, S. Biggs, O.J. Cayre, D. Harbottle, Polymer Molecular Weight Dependence on Lubricating Particle-Particle Interactions, *Ind Eng Chem Res* 57(6) (2018) 2131-2138.
- [50] M. Raftari, Z.Y.J. Zhang, S.R. Carter, G.J. Leggett, M. Geoghegan, Salt Dependence of the Tribological Properties of a Surface-Grafted Weak Polycation in Aqueous Solution, *Tribol Lett* 66(1) (2018).
- [51] Z.Y. Zhang, A.J. Morse, S.P. Armes, A.L. Lewis, M. Geoghegan, G.J. Leggett, Nanoscale Contact Mechanics of Biocompatible Polyzwitterionic Brushes, *Langmuir* 29(34) (2013) 10684-10692.
- [52] C. LoPresti, M. Massignani, C. Fernyhough, A. Blanzs, A.J. Ryan, J. Madsen, N.J. Warren, S.P. Armes, A.L. Lewis, S. Chirasatitsin, A.J. Engler, G. Battaglia, Controlling Polymersome Surface Topology at the Nanoscale by Membrane Confined Polymer/Polymer Phase Separation, *ACS Nano* 5(3) (2011) 1775-1784.
- [53] V.J. Verruto, R.K. Le, P.K. Kilpatrick, Adsorption and Molecular Rearrangement of Amphoteric Species at Oil-Water Interfaces, *J Phys Chem B* 113(42) (2009) 13788-13799.

- [54] S. Barman, G.F. Christopher, Role of capillarity and microstructure on interfacial viscoelasticity of particle laden interfaces, *J Rheol* 60(1) (2016) 35-45.
- [55] S. Adams, W.J. Frith, J.R. Stokes, Influence of particle modulus on the rheological properties of agar microgel suspensions, *J Rheol* 48(6) (2004) 1195-1213.
- [56] A. Maestro, O.S. Deshmukh, F. Mugele, D. Langevin, Interfacial Assembly of Surfactant-Decorated Nanoparticles: On the Rheological Description of a Colloidal 2D Glass, *Langmuir* 31(23) (2015) 6289-6297.
- [57] V. Trappe, D.A. Weitz, Scaling of the viscoelasticity of weakly attractive particles, *Phys Rev Lett* 85(2) (2000) 449-452.
- [58] A. Wang, W.B. Rogers, V.N. Manoharan, Effects of Contact-Line Pinning on the Adsorption of Nonspherical Colloids at Liquid Interfaces, *Phys Rev Lett* 119(10) (2017).
- [59] A. Wang, R. McGorty, D.M. Kaz, V.N. Manoharan, Contact-line pinning controls how quickly colloidal particles equilibrate with liquid interfaces, *Soft Matter* 12(43) (2016) 8958-8967.